Supporting Information: Large exciton-driven linear and nonlinear optical processes and band nesting in monolayers of nitrogen arsenide and nitrogen antimonide

Unknown Author(s)*

E-mail: luigi@luigicigarini.me

References

(1) Zhang, G.; Chaves, A.; Huang, S.; Wang, F.; Xing, Q.; Low, T.; Yan, H. Determination of layer-dependent exciton binding energies in few-layer black phosphorus. *Sci. Adv.* **2018**, *4*, 9977.

(2) Youngblood, N.; Peng, R.; Nemilentsau, A.; Low, T.; Li, M. Layer-Tunable Third-Harmonic Generation in Multilayer Black Phosphorus. *ACS Photonics* **2017**, *4*, 8.

(3) He, K.; Kumar, N.; Zhao, L.; Wang, Z.; Mak, K. F.; Zhao, H.; Shan, J. Tightly Bound excitons in monolayer WSe_2. *Phys. Rev. Lett.* **2014**, *113*, 026803.

(4) Arora, A.; Koperski, M.; Nogajewski, K.; Marcus, J.; Faugerasa, C.; Potemski, M.

Table S1: Reported experimental quasi-particle direct band-gap, fundamental exciton binding energy (BE), linewidth (LW) and nonlinear coefficients (at excitation wavelength in nm) in various supported materials, including this work. Notations: c = chemical vapor deposition, e = mechanical exfoliation, m = molecular beam epitaxy, L = layer, PDMS = polydimethylsiloxane, rt = room temperature (300 K), $\oslash$ = temperature not mentioned, $*$ = this work, † = *ab-initio*, comm = commercial, encap = encapsulation, CV(P)T = chemical vapor(pressure) transport and blank space = not reported. Values available at other than 300 K are specifically mentioned.

Material	Substrate	rt Band -gap (eV)	rt BE (eV)	rt LW (meV)	$\lvert\chi^{(2)}\rvert$(λnm) (pm/V)	$\lvert\chi^{(3)}\rvert$(λnm) $\left(10^{-19}\,\frac{m^2}{V^2}\right)$
BP (4L)	PDMS	0.84 [1]	0.139 [1]	20 [1]		
BP (29L)	SiO_2/Si					1.4(1557) [2]
ML WSe_2	SiO_2/Si(e)	2.02 [3]	0.37 [3]	50 [4]	16.5(1560) [5]	1(1560) [5]
	Sapphire	1.89$^{\oslash}$ [6]	0.240$^{\oslash}$ [6]			
	Au	1.75$^{\oslash}$ [6]	0.140$^{\oslash}$ [6]			
	SiO_2/Si(e)	2.63(4-300 K) [7]	0.887(4-300 K) [7]			
	hBN encap (comm) [8]			3.9-4.2(4 K)		
				32-34(292 K)		
	Quartz(e)			∼13(160 K) [9]		
	Si/SiO_2/(e)				1×10^4(816) [10]	
ML MoS_2	Fused silica(e)	2.17±0.1 [11]	0.31±0.04 [11]		160(810) [12]	
	SiO_2/Si(e)				1×10^5(810) [13]	3.6(1560) [5]
	Sapphire$^{\oslash}$	2.11 [6]	0.240 [6]			
	Si/SiO_2(c)				6 [14]	
	Si/SiO_2(c)				5×10^3(816) [13]	
	amorphous quartz(e)				30-100(680-1080) [15]	
	Au	1.9$^{\oslash}$ [6]	0.090$^{\oslash}$ [6]			
	hBN/Fused silica(e)	2.47±0.08 [16]	0.44±0.08$^{\triangle}$ [16]			
	isolated†			44 [17]		
	HOPG(c)	2.15±0.06(77 K) [18]	0.2(77 K) [18]			
	HOPG(c)	2.15±0.1(77 K) [19]	∼0.3(77 K) [19]			
	hBN encap (comm) [8]			2.0-4.5(4 K)		
				44-46(292 K)		
	hBN encap (CPT) [8]			3.9-5.0(4 K)		
				44-49(292 K)		
ML $MoSe_2$	Si/SiO_2(e)		0.1(5 K) [20]	40 [21]	37(1560) [5]	2.2(1560) [5]
	6H-SiC(0001)(m)	1.58(40 K) [22]				
	hBN encap (VPT) [8]			2.4-4.9(4 K)		
				34-36(292 K)		
	hBN encap(m)			6.6(4 K) [23]		
	Si/SiO_2(c)				50(1200-1800) [24]	
ML $MoTe_2$	Si/SiO_2(e)		0.540(10 K) [25]			
ML WS_2	suspended and Si/SiO_2(c)$^{\oslash}$				9×10^3(832) [26]	
	SiO_2/Si(e)	2.14±0.04(5 K)	0.32±0.04(5 K)			
	Si/SiO_2(e)				16.2(1560) [5]	2.4(1560) [5]
	SiO_2(c)	2.31–2.53 [27]	0.26–0.48 [27]			
	SiO_2/Si(e)	2.73 [28]	0.71±0.01 [28]			
	SiO_2/Si(e)	3.01(4-300 K) [7]	0.929(4-300 K) [7]			
	Fused silica(e)	2.33±0.05 [16]	0.32±0.05 [16]			
	Fused quartz(e)	2.38±0.06 [11]	0.360±0.060 [11]			
	Si/SiO_2(e)			24 [21]		
	hBN encap (comm) [8]			4.3-4.8(4 K)		
				23-25(292 K)		
	Sapphire(c)			5.96(10 K) [29]		
ML InSe	hBN(e)	2.9(100 K) [30]				
	hBN encap(e)				223±138(810) [31]	
	at 300 K					
ML GaSe	Si/SiO_2(c)				2.4×10^3 [32]	
ML hBN	Fused silica(e)				10(810) [12]	
	Graphite(m)	6.1 [33]	1.9 [33]	32(10 K)-38(300 K) [33]		
	isolated† [34]	7.36	1.81	97(0 K)-260(300 K)		
hBN (110±2L)	SiO_2(e)				42(810) [35]	
ML NP*	isolated†	4.92	2	151	800(364)	14(539)

*We note the ML NP direct-DFT gap to be about 2.63 eV. At 300 K, this reduces to 2.61 eV. The GW correction is further added to obtain the resultant quasi-particle direct gap at 300 K.
$^{\triangle}$Obtained by analyzing the B-excitonic transition state.

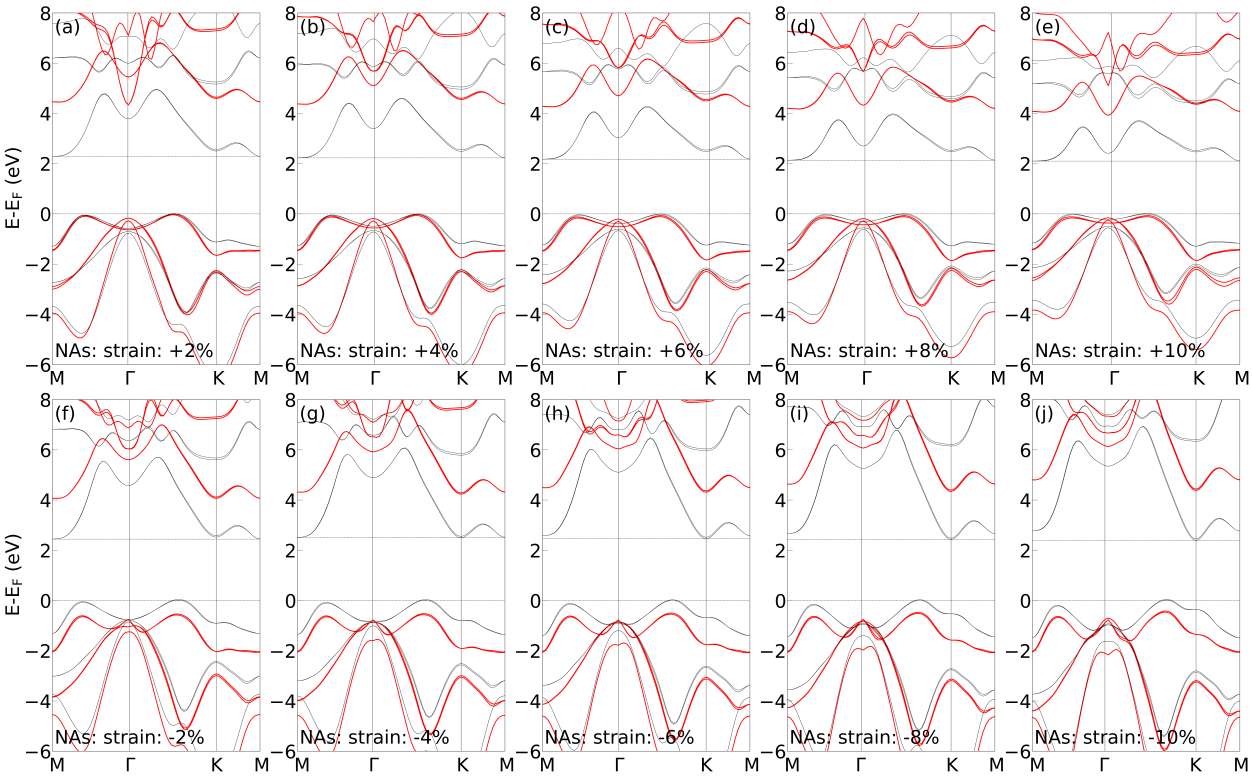

Figure 1: Ground state (grey) and G_0W_0 (red) band structure of monolayer NAs under various biaxial (a)-(e) tensile and (f)-(g) compressive strains respectively.

Excitonic resonances in thin films of WSe_2: from monolayer to bulk material. *Nanoscale* **2015**, *7*, 10421.

(5) Autere, A.; Jussila, H.; Marini, A.; Saavedra, J. R. M.; Dai, Y.; Säynätjoki, A.; Karvonen, L.; Yang, H.; Amirsolaimani, B.; *et al.*, R. A. N. Optical harmonic generation in monolayer group-VI transition metal dichalcogenides. *Phys. Rev. B* **2018**, *98*, 115426.

(6) Park, S.; Mutz, N.; Schultz, T.; Blumstengel, S.; Han, A.; Aljarb, A.; Li, L.-J.; List-Kratochvil, E. J. W.; Amsalem, P.; Koch, N. Direct determination of monolayer MoS_2 and WSe_2 exciton binding energies on insulating and metallic substrate. *2D Mater.* **2018**, *5*, 025003.

(7) Hanbickia, A.; Curriea, M.; Kioseogloub, G.; Friedmana, A.; Jonker, B. Measurement of high exciton binding energy in the monolayer transition-metal dichalcogenides $WS_2$and WSe_2. *Solid State Commun.* **2015**, *203*, 16.

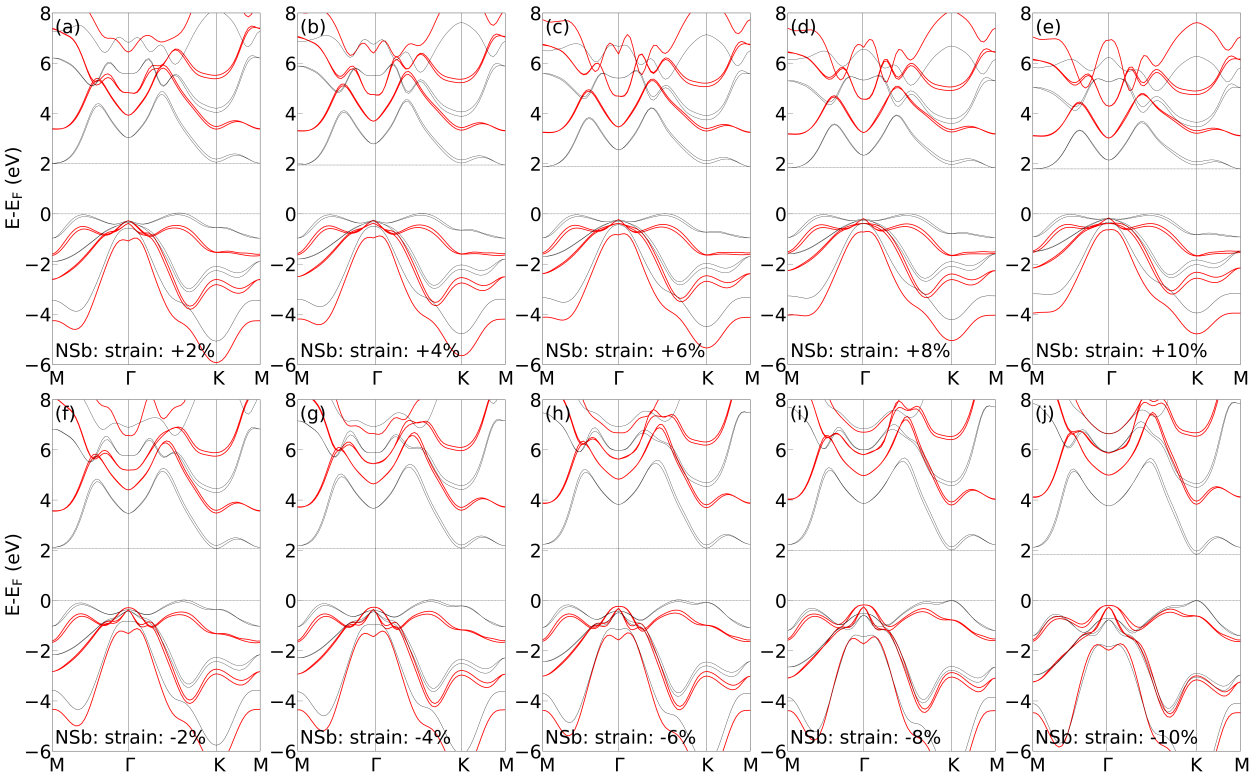

Figure 2: Ground state (grey) and G_0W_0 (red) band structure of monolayer NSb under various biaxial (a)-(e) tensile and (f)-(g) compressive strains respectively.

(8) Cadiz, F.; Courtade, E.; Robert, C.; Wang, G.; Shen, Y.; Cai, H.; Taniguchi, T.; Watanabe, K.; Carrere, H.; *et al.*, D. L. Excitonic linewidth approaching the homogeneous limit in MoS_2-based van der Waals heterostructures. *Phys. Rev. X* **2017**, *7*, 021026.

(9) Miyauchi, Y.; Konabe, S.; Wang, F.; Zhang, W.; Hwang, A.; Hasegawa, Y.; Zhou, L.; Mouri, S.; Toh, M.; Eda, G.; Matsuda, K. Evidence for line width and carrier screening effects on excitonic valley relaxation in 2D semiconductors. *Nat. Comm.* **2018**, *9*, 2598.

(10) Ribeiro-Soares, J.; Janisch, C.; Liu, Z.; Elías, A. L.; Dresselhaus, M. S.; Terrones, M.; Cançado, L. G.; Jorio, A. Second harmonic generation in WSe_2. *2D Mater.* **2015**, *2*, 045015.

(11) Rigosi, A. F.; Hill, H. M.; Rim, K. T.; Flynn, G. W.; Heinz, T. F. Electronic band gaps and exciton binding energies in monolayer $Mo_xW_{1-x}S_2$ transition metal dichalcogenide

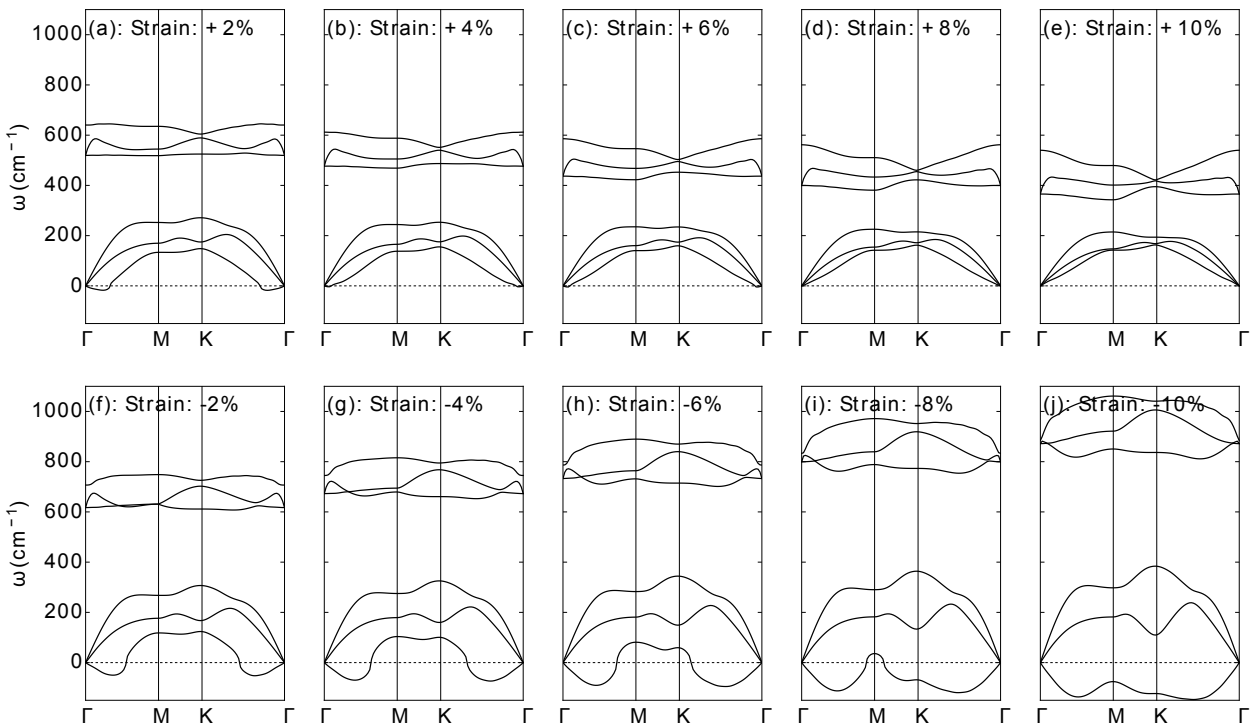

Figure 3: Phonon dispersion in monolayer NAs for biaxial (a)-(e) tensile and (f)-(g) compressive strains respectively.

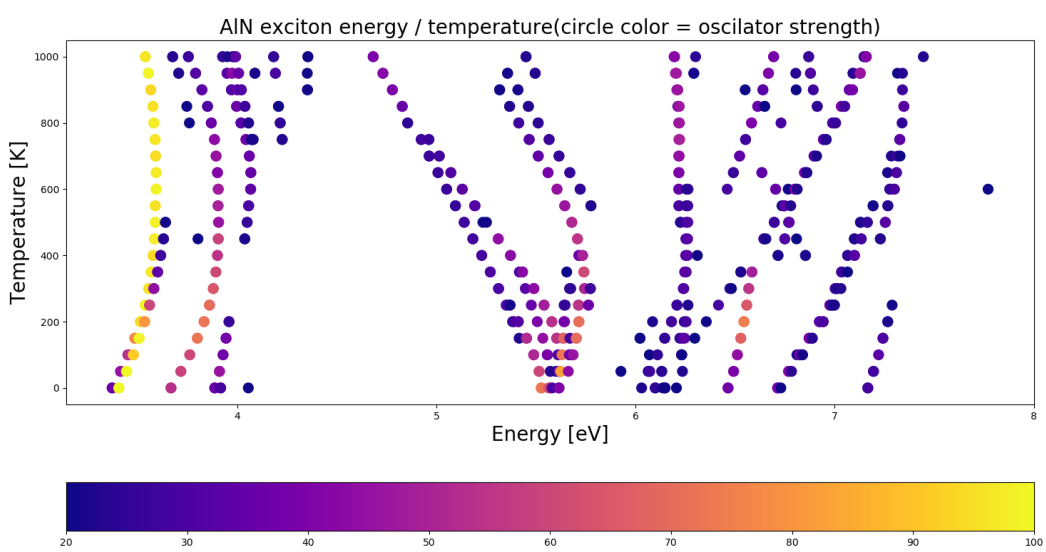

Figure 4: Calculated Excitonic energies showed as functions of temperature.

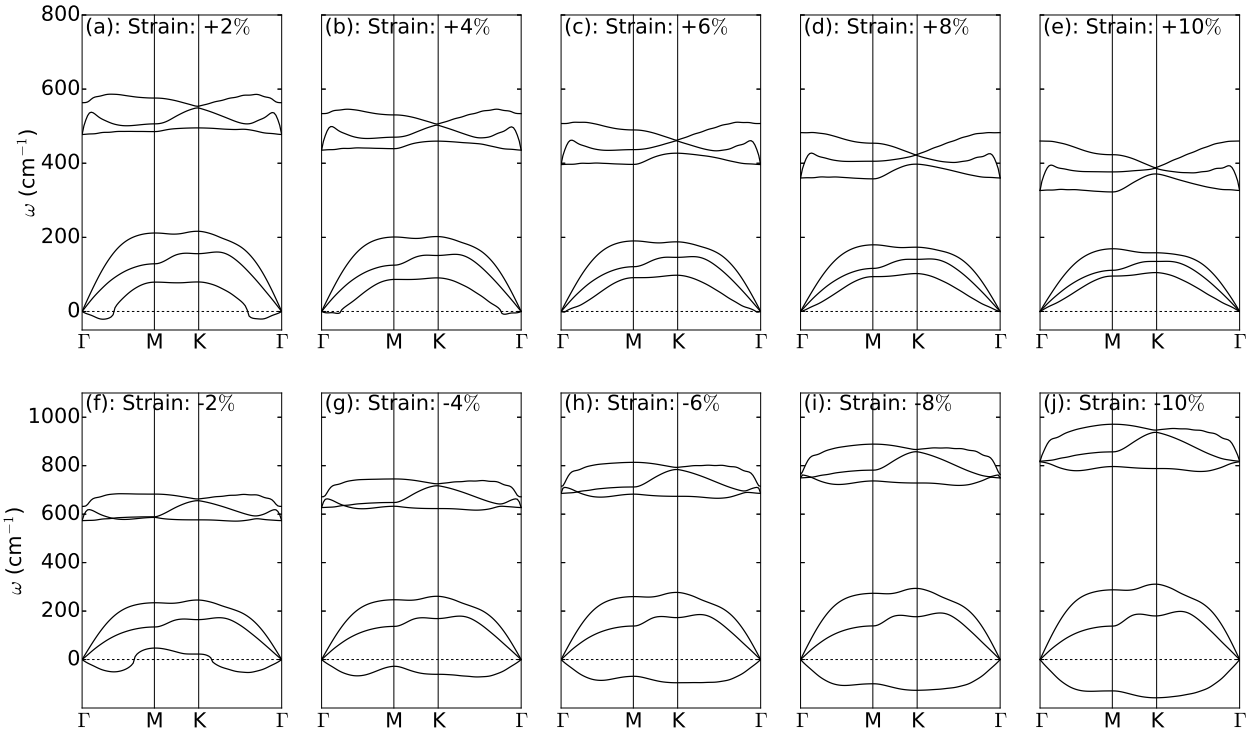

Figure 5: Phonon dispersion in monolayer NSb for biaxial (a)-(e) tensile and (f)-(g) compressive strains respectively.

alloys probed by scanning tunneling and optical spectroscopy. *Phys. Rev. B* **2016**, *94*, 075440.

(12) Li, Y.; Rao, Y.; Mak, K. F.; You, Y.; Wang, S.; Dean, C. R.; Heinz, T. F. Probing symmetry properties of few layer MoS_2 and h-BN by optical second-harmonic generation. *Nano Lett.* **2013**, *13*, 3329.

(13) Kumar, N.; Najmaei, S.; Cui, Q.; Ceballos, F.; Ajayan, P. M.; Lou, J.; Zhao, H. Second harmonic microscopy of monolayer MoS_2. *Phys. Rev. B* **2013**, *87*, 161403(R).

(14) Clark, D. J.; Senthilkumar, V.; Le, C. T.; Weerawarne, D. L.; Shim, B.; Jang, J. I.; Shim, J. H.; Cho, J.; Sim, Y.; *et al.*, M.-J. S. Strong optical nonlinearity of CVD-grown MoS_2 monolayer as probed by wavelength-dependent second-harmonic generation. *Phys. Rev.B* **2014**, *90*, 121409(R).

(15) Malard, L. M.; Alencar, T. V.; Barboza, A. P. M.; Mak, K. F.; de Paula, A. M.

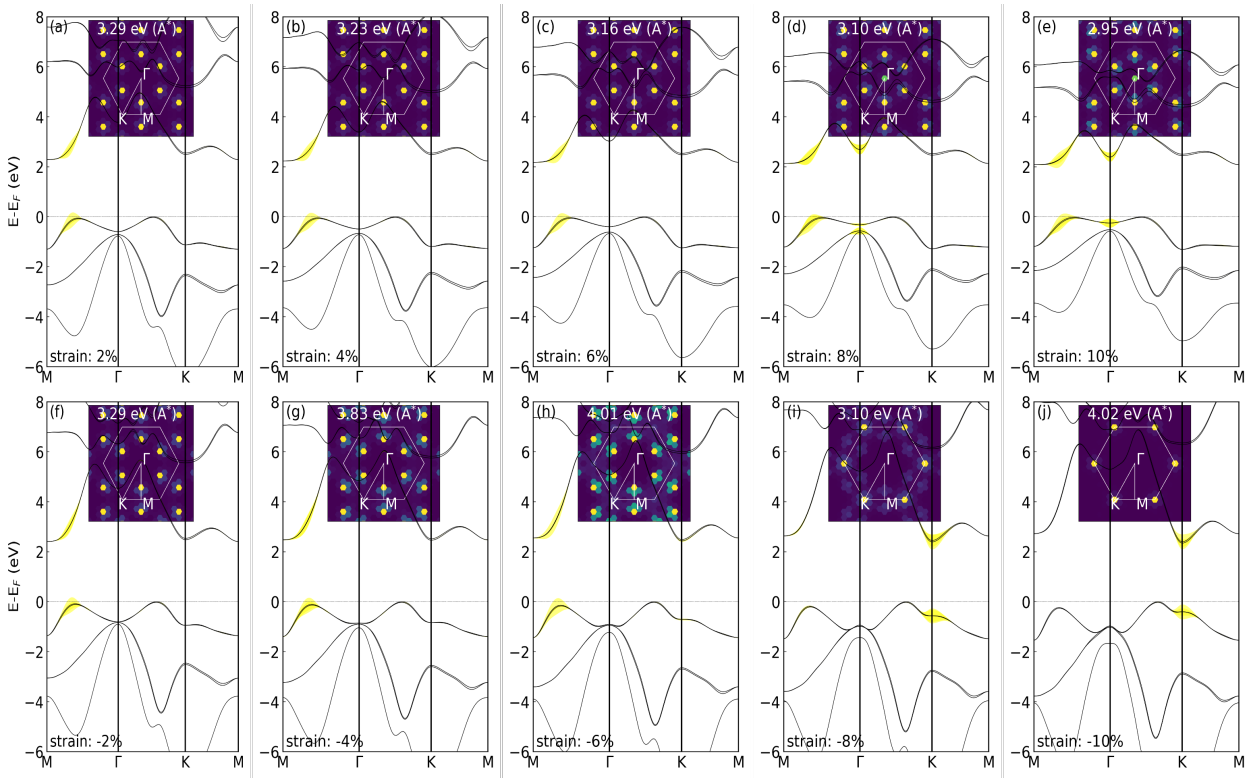

Figure 6: Excitonic weights showing the most important electronic transitions along the high symmetry points of the BZ of monolayer NAs under biaxial (a)-(e) tensile and (f)-(g) compressive strains respectively.

Observation of intense second harmonic generation from MoS_2 atomic crystals. *Phys. Rev. B* **2013**, *87*, 201401(R).

(16) Hill, H. M.; Rigosi, A. F.; Roquelet, C.; Chernikov, A.; C.Berkelbach, T.; Reichman, D. R.; Hybertsen, M. S.; Brus, L. E.; Heinz, T. F. Observation of excitonic Rydberg states in monolayer $MoS_2$and WS_2 by photoluminescence excitation spectroscopy. *Phys. Rev. B* **2015**, *15*, 2992.

(17) Molina-Sànchez, A.; Palummo, M.; Marini, A.; Wirtz, L. Temperature-dependent excitonic effects in the optical properties of single-layer MoS_2. *Phys. Rev. B* **2016**, *93*, 155435.

(18) Zhang, C.; Johnson, A.; Hsu, C.-L.; Li, L.-J.; Shih, C.-K. Direct imaging of band profile

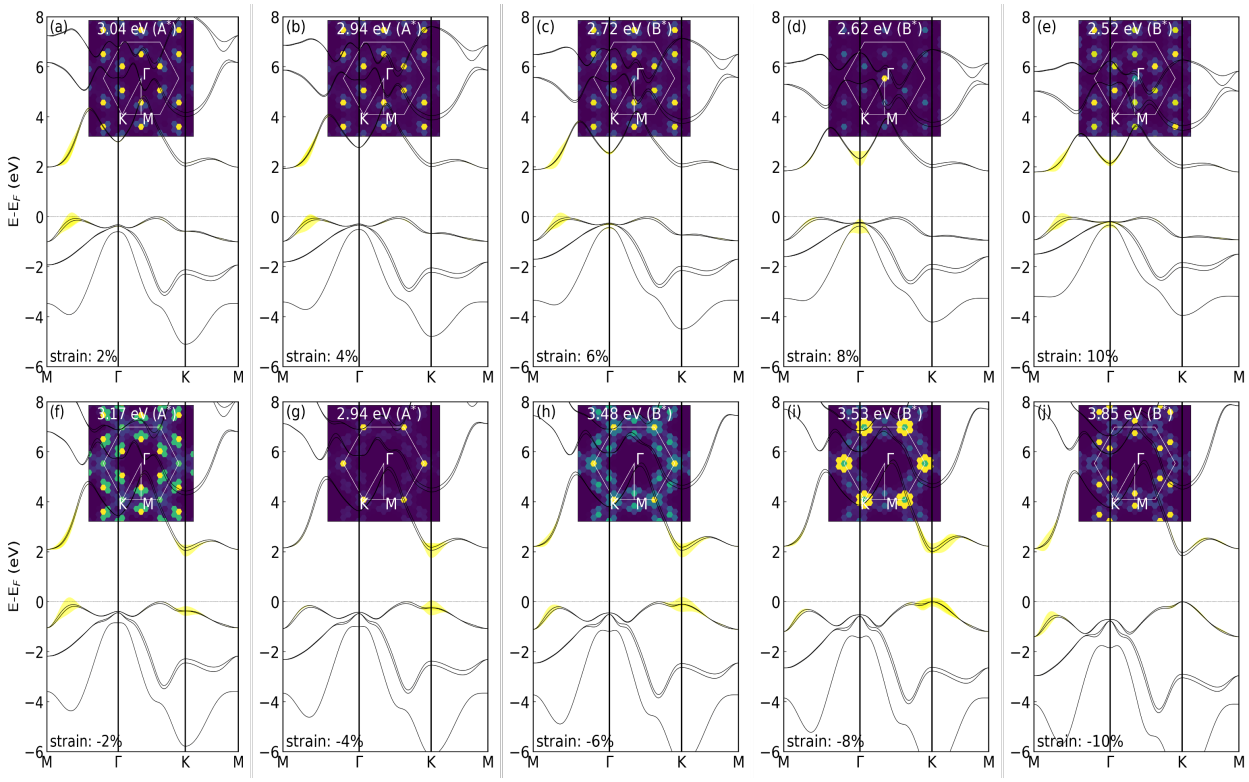

Figure 7: Excitonic weights showing the most important electronic transitions along the high symmetry points of the BZ of monolayer NSb under biaxial (a)-(e) tensile and (f)-(g) compressive strains respectively.

in single layer MoS_2 on Graphite: quasiparticle energy gap, metallic edge states, and edge band bending. *Nano Lett.* **2014**, *14*, 2443.

(19) Chiu, M.-H.; Zhang, C.; Shiu, H.-W.; Chuu, C.-P.; Chen, C.-H.; Chang, C.-Y. S.; Chen, C.-H.; Chou, M.-Y.; Shih, C.-K.; Li, L.-J. Determination of band alignment in the single-layer MoS_2/WSe_2 heterojunction. *Nat. Comm.* **2015**, *6*, 7666.

(20) Arora, A.; Nogajewski, K.; Molas, M.; Koperskiab, M.; Potemski, M. Exciton band structure in layered $MoSe_2$: from a monolayer to the bulk limit. *Nanoscale* **2015**, *7*, 20769.

(21) Selig, M.; Berghäuser, G.; Raja, A.; Nagler, P.; Schüller, C.; Heinz, T. F.; Korn, T.; Chernikov, A.; Malic, E.; Knorr, A. Excitonic linewidth and coherence lifetime in monolayer transition metal dichalcogenides. *Nat. Comm.* **2016**, *7*, 13279.

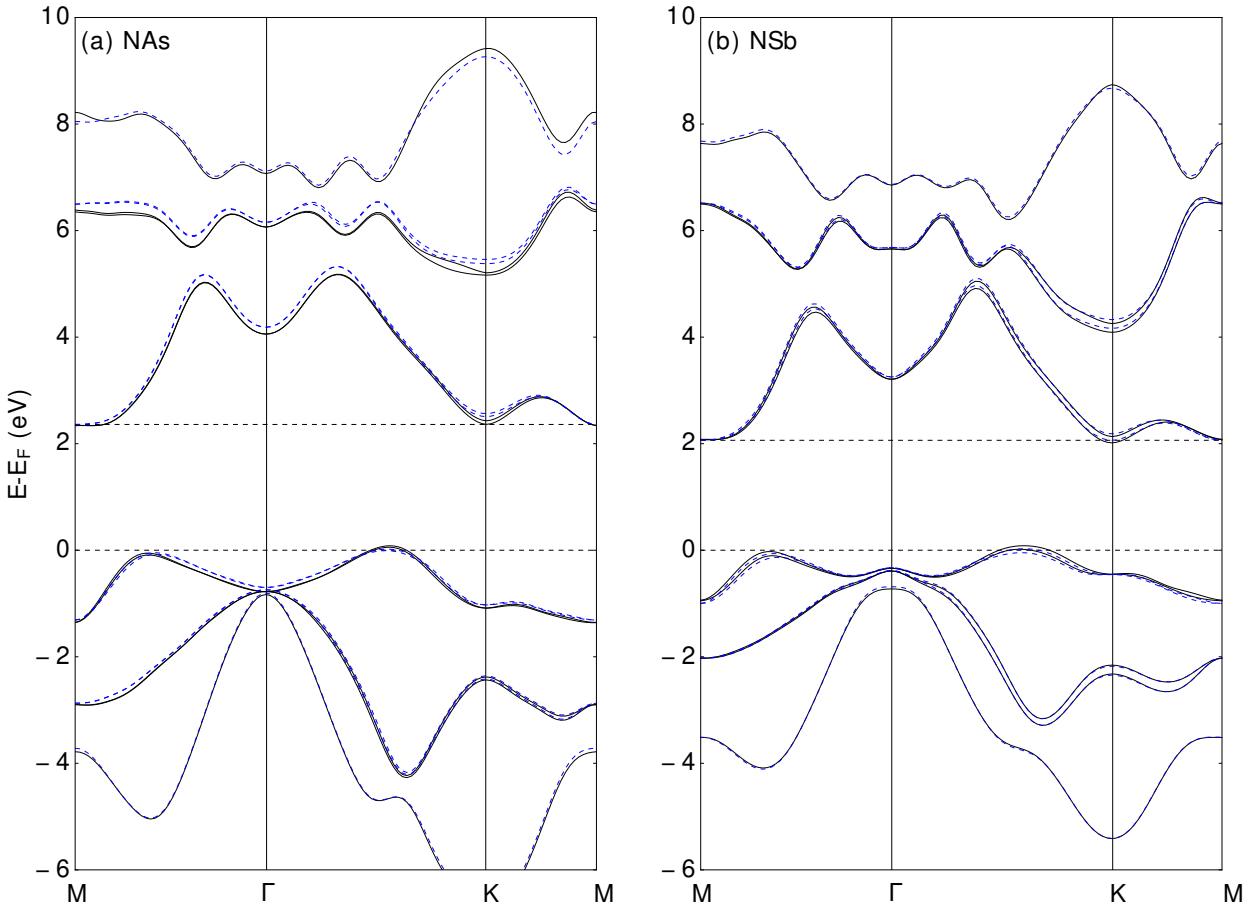

Figure 8: Zero point electronic dispersion of (a) NAs and (b) NSb monolayers. The dotted lines are the frozen atom band structure.

(22) Zhang, Y.; Chang, T.-R.; Zhou, B.; Cui, Y.-T.; Yan, H.; Liu, Z.; Schmitt, F.; Lee, J.; Moore, R.; *et al.*, Y. C. Direct observation of the transition from indirect to direct bandgap in atomically thin epitaxial $MoSe_2$. *Nat. Nanotechnol.* **2014**, *9*, 111.

(23) Pacuski, W.; Grzeszczyk, M.; Nogajewski, K.; Bogucki, A.; Oreszczuk, K.; Kucharek, J.; Połczyńska, K. E.; Seredyński, B.; Rodek, A.; *et al.*, R. B. Narrow excitonic lines and large-scale homogeneity of transition-metal dichalcogenide monolayers grown by molecular beam epitaxy on hexagonal boron nitride. *Nano Lett.* **2020**, *20*, 3058.

(24) Le, C. T.; Clark, D. J.; Ullah, F.; Senthilkumar, V.; Jang, J. I.; Sim, Y.; Seong, M.-J.; Chung, K.-H.; Park, H.; Kim, Y. S. Nonlinear optical characteristics of monolayer $MoSe_2$. *Ann. Phys.* **2016**, *528*, 551.

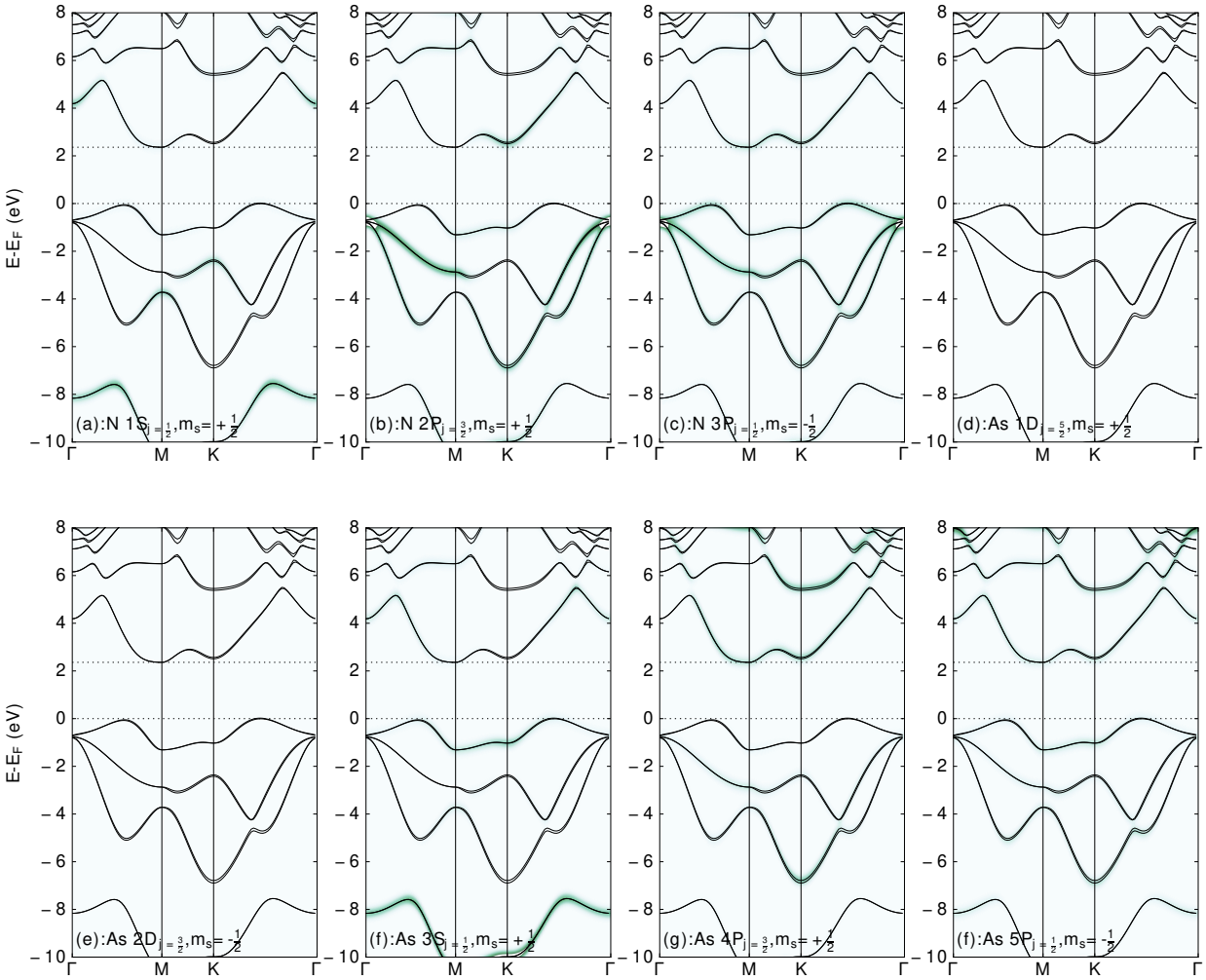

Figure 9: Bare electronic dispersion of NAs monolayer showing the partial density of states projected on the former. The contour plots exhibits the partial occupancy of (a) nitrogen $1S_{j=\frac{1}{2}}$, m_s=$\frac{1}{2}$, (b) nitrogen $2P_{j=\frac{3}{2}}$, m_s=$\frac{1}{2}$, (c) nitrogen $3P_{j=\frac{1}{2}}$, m_s=$-\frac{1}{2}$, (d) arsenic $1D_{j=\frac{5}{2}}$, m_s=$\frac{1}{2}$, (e) arsenic $2D_{j=\frac{3}{2}}$, m_s=$\frac{1}{2}$, (f) arsenic $3S_{j=\frac{1}{2}}$, m_s=$\frac{1}{2}$, (g) arsenic $4P_{j=\frac{3}{2}}$, m_s=$+\frac{1}{2}$ and (h) arsenic $5P_{j=\frac{1}{2}}$, m_s=$-\frac{1}{2}$.

(25) Robert, C.; Picard, R.; Lagarde, D.; Wang, G.; Echeverry, J. P.; Cadiz, F.; Renucci, P.; Högele, A.; Amand, T.; *et al.*, X. M. Excitonic properties of semiconducting monolayer and bilayer $MoTe_2$. *Phys. Rev. B* **2016**, *94*, 155425.

(26) Janisch, C.; Wang, Y.; Ma, D.; Mehta, N.; Elías, A. L.; Perea-López, N.; Terrones, M.; Crespi, V.; Liu, Z. Extraordinary second harmonic generation in tungsten disulfide monolayers. *Sci. Rep.* **2014**, *4*, 5530.

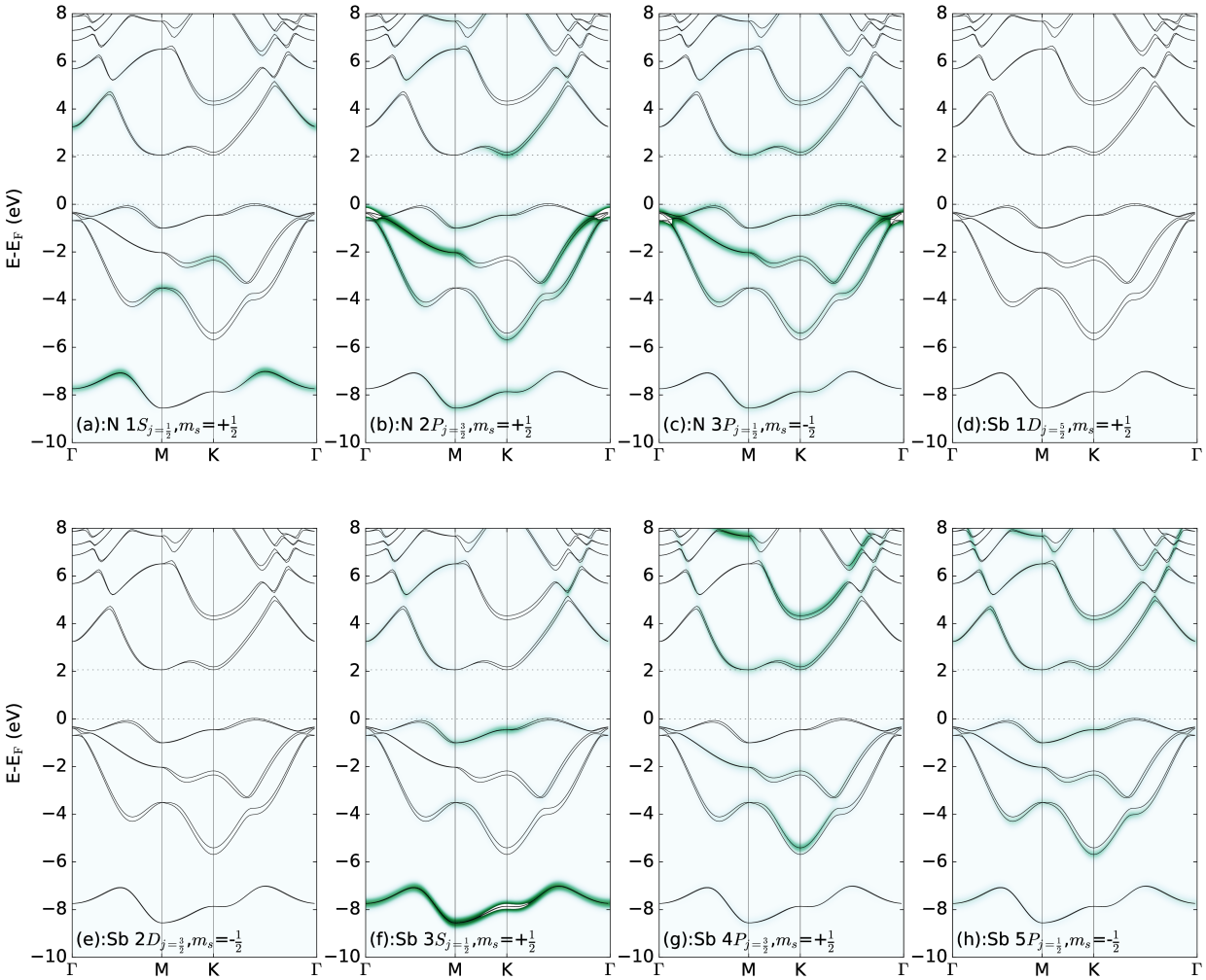

Figure 10: Bare electronic dispersion of NSb monolayer showing the partial density of states projected on the former. The contour plots exhibits the partial occupancy of (a) nitrogen $1S_{j=\frac{1}{2}}$, m_s=$\frac{1}{2}$, (b) nitrogen $2P_{j=\frac{3}{2}}$, m_s=$\frac{1}{2}$, (c) nitrogen $3P_{j=\frac{1}{2}}$, m_s=$-\frac{1}{2}$, (d) antimony $1D_{j=\frac{5}{2}}$, m_s=$\frac{1}{2}$, (e) antimony $2D_{j=\frac{3}{2}}$, m_s=$\frac{1}{2}$, (f) antimony $3S_{j=\frac{1}{2}}$, m_s=$\frac{1}{2}$, (g) antimony $4P_{j=\frac{3}{2}}$, m_s=$+\frac{1}{2}$ and (h) antimony $5P_{j=\frac{1}{2}}$, m_s=$-\frac{1}{2}$.

(27) Stier, A. V.; M, K.; McCreary,; Jonker, B. T.; Kono, J.; Crooker, S. A. Exciton diamagnetic shifts and valley Zeeman effects in monolayer WS_2 and MoS_2 to 65 Tesla. *Nat. Comm.* **2016**, *7*, 10643.

(28) Zhu, B.; Chen, X.; Cui, X. Exciton binding energy of monolayer WS_2. *Sci. Rep.* **2015**, *5*, 9281.

(29) Guo, L.; Chen, C.-A.; Zhang, Z.; Monahan, D. M.; Lee, Y.-H.; Fleming, G. R. Line-

shape characterization of excitons in monolayer WS_2 by two-dimensional electronic spectroscopy. *Nanoscale Adv.* **2020**, *2*, 2333.

(30) Hamer, M. J.; Zultak, J.; Tyurnina, A. V.; Zólyomi, V.; Terry, D.; Barinov, A.; Garner, A.; Donoghue, J.; Rooney, A. P.; *et al.*, V. K. Indirect to direct gap crossover in two-dimensional InSe revealed by angle-resolved photoemission spectroscopy. *ACS Nano* **2019**, *13*, 2136.

(31) Leisgang, N.; Roch, J. G.; Froehlicher, G.; Hamer, M.; Terry, D.; Gorbachev, R.; Warburton, R. J. Optical second harmonic generation in encapsulated single-layer InSe editors-pick. *AIP Adv.* **2018**, *8*, 105120.

(32) Zhou, X.; Cheng, J.; Zhou, Y.; Cao, T.; Hong, H.; Liao, Z.; Wu, S.; Peng, H.; Liu, K.; Yu, D. Strong second-harmonic generation in atomic layered GaSe. *J. Am. Chem. Soc.* **2015**, *137*, 7994.

(33) Elias, C.; Valvin, P.; Pelini, T.; Summerfield, A.; Mellor, C.; Cheng, T.; Eaves, L.; Foxon, C.; Beton, P.; *et al.*, S. N. Direct band-gap crossover in epitaxial monolayer boron nitride. *Nat. Comm.* **2019**, *10*, 2639.

(34) Mishra, H.; Bhattacharya, S. Giant exciton-phonon coupling and zero-point renormalization in hexagonal monolayer boron nitride. *Phys. Rev. B* **2019**, *99*, 165201.

(35) Kim, S.; Fröch, J. E.; Gardner, A.; Li, C.; Aharonovich, I.; Solntsev, A. S. Second-harmonic generation in multilayer hexagonal boron nitride flakes. *Opt. Lett.* **2019**, *44*, 5792.